12-12-2022

Nucleation-accumulation Mode Trade-off in Non-volatile Particle Emissions From a Small Non-road Small Diesel Engine

Indranil Brahma
ib011@bucknell.edu

Odinmma John-Paul Ofili
Bucknell University

Recommended Citation

Brahma, I., Ofili, O. Nucleation-accumulation mode trade-off in non-volatile particle emissions from a small non-road small diesel engine. Environ Sci Pollut Res 29, 89449–89468 (2022). https://doi.org/10.1007/s11356-022-22032-w

Nucleation-Accumulation Mode Trade-Off in Non-Volatile Particle Emissions from a Small Non-Road Small Diesel Engine

Indranil Brahma* and Odinmma Ofili

Department of Mechanical Engineering, Bucknell University, USA

*Corresponding Author: Indranil Brahma, ib011@bucknell.edu

Keywords: Particle Emissions, Diesel Engine, Non-Road Engine, Nanoparticles, Nucleation Mode, Accumulation Mode

Acknowledgements: The authors gratefully acknowledge the financial support of the US National Science Foundation the resources provided by Bucknell University for this work.

Abstract: Small (<8kW) non-road engines are a significant source of pollutants such as particle number (PN) emissions. Many small non-road engines do not have diesel particulate filters (DPFs). They are so designed that air-fuel ratio (AFR) can be adjusted to control visible diesel smoke and particulate matter (PM) resulting from larger accumulation mode particles. However, the effect of AFR variation on smaller nucleation mode nanoparticle emissions is not well understood. Several studies on larger engines have reported a trade-off between smaller and larger particles. In this study, AFR was independently varied over the entire engine map of a naturally aspirated (NA) non-road small diesel engine using forced induction (FI) of externally compressed air. AFR's ranged from 57-239 compared to the design range of 23-92 for the engine, including unusually high AFR's at full-load operation, not previously reported for conventional combustion. As expected, larger accumulation mode particles were lowered (up to 15 times) for FI operation. However, the smaller nucleation mode nanoparticles increased up to 15 times. Accumulation mode particles stopped decreasing above an AFR threshold while nucleation particles continuously increased. In-cylinder combustion analysis showed a slightly smaller ignition delay and higher burn rate for FI cases relative to NA operation. Much higher peak cylinder pressures were accompanied by much lower combustion and exhaust gas temperatures (EGT), due to higher in-cylinder mass during FI operation. Peak nucleation mode emissions were shown to be negatively correlated to EGT for all the data, collapsing on a single curve. This is consistent with some other studies reporting increased nucleation mode emissions (and higher accumulation mode particles) with decreased load, lower speed, lower EGR, advanced combustion phasing and higher injection pressure, all of which reduce EGT. The nucleation-accumulation trade-off has been explained by the 'adsorption hypothesis' by some investigators. In the current work, an alternative/supplemental argument has been made for the possibility that lower cylinder temperatures during the late-burning phase (correlated to lower EGT) phase hampers oxidation of nucleation mode particles and increases nucleation mode emissions.

1.Introduction: Although automotive engineers routinely use air-fuel ratio (AFR) to reduce particulate matter (PM) over engine drive cycles or to control smoke spikes during dynamic operation (Brahma 2012 a, b, 2013), they primarily rely on diesel particulate filters (DPFs) to meet PM emission targets. In contrast, the smallest non-road engines generally do not have DPFs and engineers rely on AFR (either through adjustment or design) to control smoke/PM. The smallest engine category for non-road diesel engines defined by the US Environmental Protection Agency is < 8 kW. Currently applicable tier-4 standards (US EPA Tier 4 ruling 2004) require PM emission below 0.4 g/kW-hr for the smallest diesel off-road engines, (0.6 g/kW-hr for hand-starting engines) as compared to 0.03 g/kW-hr or lower for engines > 19 kW. Some small engines, e.g. air-cooled industrial diesel engines below 8 kW currently meet these standards without DPF technology. In such cases AFR plays a vital role in PM control. At any given engine speed, the maximum power of naturally aspirated diesels is limited by diesel smoke or particulate mass limits. Since the air flow rate remains nearly constant, the air-fuel ratio (AFR) is constrained by setting an upper limit on the mass of fuel injected per stroke. For a turbocharged engine, the AFR can be limited by adjusting both fuel as well as air flow rate. However, the effect of AFR on particle number (PN) emissions is not well studied. The limited literature on the subject, mostly from automotive engines, suggests that decreasing particulate mass might inadvertently increase PN. The current work explores this possibility for small non-road diesel engines by changing AFR using external compressed air. The literature is reviewed shortly after further elaboration of this motivation.

Particle emissions from diesel engines usually form a bi-modal and sometimes tri-modal distribution. The smallest particles below 50 nm typically constitute more than 90% of particle number and less than 20% of particle mass. These small particles are formed from nucleation of volatile organic compounds, Sulphur compounds and metallic compounds as well as solid carbon. They and are collectively known as 'nucleation mode' particles (Kittelson 1998). The second mode comprises of larger particles typically between 100-1000 nm. Most of the particle mass is concentrated within the 100-300 nm range (Kittelson 1998). The particles in this mode are collectively termed 'accumulation mode' particles. They consist of carbonaceous agglomerates and associated adsorbed materials. Several investigations including the current work have reported an increase in nucleation mode particle number when engine operating conditions are adjusted to reduce the larger accumulation mode particles, and vice-versa. This nucleation-accumulation trade-off can also be considered a particle number (PN) versus particulate mass (PM) tradeoff, and is of primary interest in the current work. The third mode of particle size distributions is formed from accumulation particles that are deposited on engine surfaces and re-entrained to grow bigger. They are typically larger than 1000 nm and referred to as 'coarse mode' particles.

While diesel particulates have been correlated with many types of health hazards (Sydbom et al. 2001, Brunekreef & Holgate 2002, Englert 2004, Pope III et al. 2006, Ristkovski et al. 2012), the relative toxicity of nucleation versus accumulation particles is not currently well understood, and limited literature exists on the subject (Xue et al. 2019). Still, nucleation particles are of particular concern because their small size can potentially allow them to infiltrate into the blood stream through the lungs and then transported to other organs (Oberdörster et al. 2004, 2005). A recent experimental study has demonstrated that nucleation particles have a higher probability of being deposited in the human respiratory tract (Rissler et al. 2012). At the same time, a nucleation mode-accumulation mode trade-off for non-volatile particles has been reported by several investigators in response to changes in engine load, injection timing and other parameters. A recent comprehensive investigation by Reijnders et. al. (2018) has shown a consistent trade-off for 500 individual engine operating conditions generated by varying engine load, exhaust gas recirculation (EGR) fraction, injection pressure, injection timing and engine speed for a heavy-duty engine using 18 different fuels. Such trade-offs are likely to have significant health implications.

Reijnders et. al. used a heavy-duty diesel engine for their work. However, no such study exists for small diesel engines which are used for a multitude of industrial, agricultural and residential applications worldwide, particularly in regions with unreliable electricity grids. For example, a 2014 world bank report (World bank report, 2014) that seeks to quantify emissions from diesel generators in Nigeria reports that the deficit between demand (ranging between 7500-10,000 MW) and power from the grid (about 4500 MW) was largely met by gasoline and diesel generators, of which about 780 MW-1820 MW was produced by residential gensets. Though the majority of these gensets were run on subsidized gasoline, nearly 14%

of Nigerian households that reported purchasing fuel for power used diesel fuel (467,612 diesel gensets). Most small diesel engines is such situations are unlikely to have DPFs or restrictions on PN emissions. They might be calibrated to eliminate visible smoke and/or to meet particulate mass standards. But in doing so, is it possible that nanoparticle emissions might increase? The current work attempts to answer this question by systematically increasing the AFR to eliminate visible smoke and PM. Results suggest a similar trade-off between smaller and larger particles as reported by other researchers using larger engines. Hence it is possible that small diesel engines without DPF's could be a significant source of nanoparticles in close human proximity because they were calibrated to 'clean' without visible smoke using AFR adjustments. Environmental and public health policy makers should be aware of nanoparticle emissions from diesel generators and other equipment.

Note that the current study did not seek to isolate the causative effect of AFR variation by holding other all parameters constant. Changes in combustion phasing as well as injected fuel mass accompanied AFR variation, but the focus was on capturing the resulting nucleation-accumulation trade-off. A novel aspect of the current work is the extremely high AFR's achieved at full load. Most diesel engines, including turbocharged engines operate in the 15-30 AFR range at full load to maximize power while meeting the smoke limit. An AFR of 70 at full load was achieved in the current work by using externally compressed air injection and hardware changes to handle almost twice peak cylinder pressure and increased vibration. The authors could not find comparable numbers in literature for conventional diesel combustion. The initial intent was to determine if PM emissions could be significantly reduced at extremely high AFRs, given their effectiveness of conventional AFR adjustments in meeting smoke and PM limits. Surprisingly, nucleation mode particles were seen to increase continuously through this extreme increase of AFR, while accumulation mode particles decrease asymptotically after a sharp drop-off likely co-incident with the disappearance of visible smoke (smoke opacity was not measured). The data is available upon request, and could be useful for understanding and modeling particle size distributions (PSDs), a relatively new area of research, see work by Duvvuri et al. (2019) for example. The relationship between nucleation mode peak fuel specific particle numbers and exhaust temperature, discussed later, is also of fundamental interest. Note that only non-volatile nucleation mode particles have been measured in the current work primarily to circumvent the measurement uncertainties associated with volatile and semi-volatile species. Such species are known to form and grow during the dilution process, and are known to depend on dilution conditions, see for example work by Khaled et. al. (1999) or Montajir et. al. (2005). Further, the impact of volatile nucleation particles in the atmosphere (in the real world outside a laboratory) is not clear. For example, Fushimi et. al. (2008) made particle measurements at a roadside and a background site 200 m away. The nucleation mode peak detected at the roadside was absent at the background site, suggesting evaporation and possible coagulation of volatile nuclei-mode particles. Hence it seems justified to attempt to eliminate volatiles and semi-volatiles in order to measure the non-volatile particles in a consistent manner.

For gasoline engines, particularly DISI engines, there exist a plethora of studies investigating the effect of independent variation of AFR on particle PSD, e.g. be He et al. (2012), probably because gasoline engine operation is much more sensitive to AFR variation than diesels. Diesel studies tend to focus on the effects of injection parameters and exhaust gas circulation, e.g. works by Bertola at al. (2001) and others (Desantes et al. 2005, Leidenberger et al. 2012, Labecki et al. 2013, Xu et al. 2014 a, b, Mohiuddin et al. 2021). There exists a significant amount of work investigating the effect of engine operating conditions on the size, structure and morphology of diesel particles, e.g. works by Zhu et al. (2005) and Lu et al. (2012). One of the earliest works relating AFR to particle morphology by Roessler et al. (1981) reported greater agglomeration and higher elemental carbon at low AFRS, and less agglomeration and higher volatile components at high AFRs. More recently, Mühlbauer et al. (2013) independently varied boost pressure, injection pressure and injection timing and measured mean particle diameter, among other things. A decreasing trend in the mean particle diameter with increasing AFR/boost as well as injecting timing was observed. Similar observations were made by Crookes et al. (2003) and Lapuerta et al. (2007). Yamada et al. (2011) analyzed exhaust from a diesel vehicle and correlated larger peaks and larger diameters for the accumulation mode to lower AFRs.

None of the above works report the effect of AFR on the entire particle size distribution (PSD). However, several recent works exploring Homogenous Charge Compression Ignition (HCCI) engines or other non-conventional combustion technologies have examined the sensitivity of the entire PSD to AFR. Kaiser et al. (2005) for example independently varied the AFR between 50-230 on an HCCI engine. The charge temperature was adjusted so that combustion started near top dead center for all cases. The accumulation mode dominated at AFR=50, peaking at around 100 nm, but was much reduced as AFR was increased. At AFR=70, the nucleation mode, which was showing modest increases with increasing AFR, suddenly spiked up as the dominant mode, and kept increasing until the maximum AFR = 230. Data was taken with and without a thermodenuder to determine the fraction of semi-volatile particles. Although about 80% of nucleation particles at AFR>85 were determined to be semi-volatile, it can be concluded from the plots presented that even solely non-volatile particles would still be the dominant (nucleation) mode at about 25 nm at some of the highest AFRs. The authors have attributed the spike in nucleation at high AFRs to incomplete combustion.

In contrast to AFR/boost/equivalence ratio sweeps, numerous studies reporting the relationship between PSDs and engine load exist. AFR is not varied independently in most of these studies but it is strongly correlated to load. These studies, e.g. work by Srivastava et al. (2011) point to a rising accumulation peak and increasing diameter at which the peak is located, when load is increased. Conversely, the nucleation mode tends to increase at low loads. This pattern has been reported for different fuels, e.g. with gas-to-liquid (GTL) fuels (Li et al. 2007) and even with gasoline engines (Gupta et al. 2010). Such a trade-off has even been reported between different engine generations; Kittelson (1998) has reported less accumulation and more nucleation particles for a newer lower emission engine relative to an older engine. The nucleation-accumulation trade-off is a consistent theme in literature.

The role of lubricating oil in particle formation, particularly nucleation mode particles, has been scrutinized in recent years. Jung, Kittelson & Zachariah (2003) dosed diesel fuel with 2% lubricating oil, and reported an order of magnitude increase in diesel particles. More recently, Pirjola et al. (2015) examined particle emissions from a turbocharged direct injection gasoline passenger car using five different lubricating oil formations (with low Sulphur gasoline) and found that lubricating oil contributed to both volatile and non-volatile emissions during acceleration and steady state operation. Transient operation was strongly influenced by lubricating oil. A positive correlation was found between metal additives and particle emissions. Similarly, Kim et al. (2020) recently reported a strong relationship between the physiochemical properties and additive constituents and particle emissions from a light duty diesel engine.

What follows is a methods section followed by a separate results and discussion section.

2. Methods: Experimental apparatus and the test plan is described in separate sub-sections.

2.1 Experimental Apparatus: High AFRs were achieved by forced induction (FI) of compressed air into a naturally aspirated (NA) engine. Figure 1 shows a schematic of apparatus. Externally compressed air at 150 PSI pressure was ducted through a pressure regulator and water separator into a 30-gallon storage tank used to supply air during FI operation. The capacitance of the storage tank ensured a steady flow rate of air to the engine irrespective of fluctuations in the building compressed air supply (supplied from a much larger storage tank that was periodically recharged by a compressor when building consumption reduced tank pressure below the lower limit). A pneumatically powered solenoid activated the three-way valve enabled the switch between the storage tank (FI operation) or the ambient air (NA operation) without interrupting engine operation.

The intake air then passed through a laminar flow element (Meriam model 50 MR2-2) where differential pressure measurements (Validyne model DP103, 5-PSI range) and boost pressure measurements (Validyne model DP 15, 20-PSI range) were made to measure fresh air flow rate. A 0.4-liter air-cooled 6.3 kW single cylinder Yanmar diesel engine (model L100EE) with a compression ratio of 20:1 was used for this study, see Table 1 for specifications.

A piezoelectric pressure transducer (PCB model 115A04) and optical crank angle encoder (BEI HS35, resolution 1^{o}) were used to measure in-cylinder pressure and crank angle respectively. Intake, exhaust and oil temperatures were measured with type-k thermocouples, and exhaust pressure was measured with a 5-psi range (Omega model PX239) transducer. Diesel fuel was conditioned at 40^{o} C using a (Brinkman Lauda model RC20) recirculating chiller heater water bath, before being supplied to the engine. Commercially available ultra-low sulfur diesel fuel was used in batches for different parts of the study outlined in the test plan, and all comparison between NA and FI particle size distributions (PSDs) have been made using the same fuel.

Engine exhaust was sampled at the exhaust port by suction into a rotating disk thermo-diluter (TSI 379020A). The sample line was an approximately 4-m long coiled copper tubing. The coil was necessary to damp the vibrations from the single-cylinder engine during FI operation, and to cool the exhaust gases from a maximum of 600^{o} C to the maximum permissible thermo-diluter temperature of 200^{o} C. The heated thermo-diluter block was maintained at 150^{0}C and hot dilution occurred at a 30:1 ratio with a constant 1.5 L/min supply of filtered particle-free dilution air. The diluted gas was then fed to a thermal conditioner (TSI 379030) where an evaporation tube maintained at 400^{o} C was used to eliminate semi-volatile matter, before secondary dilution at a 6:1 ratio. The hot dilution process was intended to reduce the partial pressure of the volatile and semi-volatile species at high temperature to eliminate nanodroplet nucleation after eventual cooldown. According to the manufacturer, TSI instruments, this combination of thermo-diluter and thermal conditioner is sufficient to meet the volatile particle removal system (VPR) specified by the UN-ECE regulation 83 covering particle measurement from light duty diesels across Europe (TSI application notes-a). The diluted gas (overall dilution ratio = 180) was then supplied to a fast particle sizer (TSI EEPS 3090) which is a differential electrical mobility spectrometer. After measurement, the gas was ported to the inlet of the exhaust fan used to ventilate the laboratory. A three-way valve at the inlet of the spectrometer allowed the measurement of ambient air periodically. Particle size distributions (PSDs) were recorded for five minutes for every engine operating condition. The last 3 minutes of this data was averaged for all results presented.

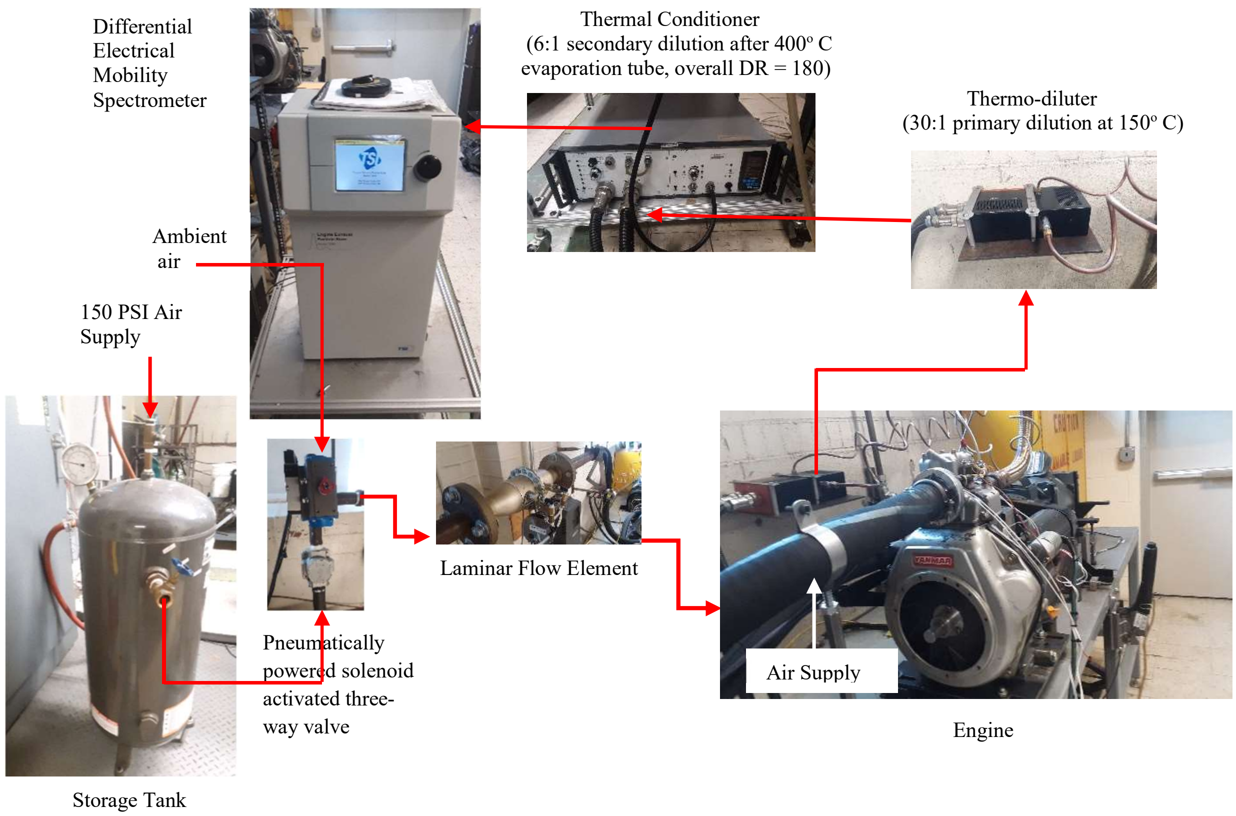

Fig 1. Experimental setup to measure particle size distributions (PSDs) while switching between naturally aspirated (NA) and forced induction (FI0 operation at the same uninterrupted engine operating condition

Table 1. Engine Specifications

Make/Model	Yanmaar/L100EE
Number of Cylinders	1
Displacement	0.418 liters
Maximum Power (continuous)	6.3 kW
Bore x Stroke	86 mm x 72 mm
Compression Ratio	20:1
Fuel Injection Timing	17° ± 0.5° bTDC
Fuel Injection Pressure	19.6 Mpa
Intake Timing (open/closed)	22.3 bTDC / 54.7 bTDC
Exhaust Timing (open/closed)	21.7 bTDC / 55.3 aTDC
Cooling System	Air Cooled
Lubricating System	Forced (Trochoid pump)
EGR System	None

2.2 Test Plan: Data was acquired for two different tests: **a.** Engine map traverse where NA and FI data was acquired for speed-load combinations spanning area under the engine torque curve and **b.** AFR sweeps at full load for different speeds using FI. Owing to fuel storage constraints, the two tests used two separate batch of fuel, but all data within each test used the same fuel. Since fuel chemistry has a strong influence on PSDs, all comparisons and trade-offs presented in this work use the same fuel.

PSDs were recorded at five different engine loads and three different engine speeds for both NA and FI operation. **Table 2** shows engine operating conditions for these 5x3x2=30 data points. The FI cases (shaded) are indicated by the 20 PSI setting in the pressure regulator column, and correspond to about 2 bar pressure intake pressure. Although not particularly high compared to turbocharged engines, the higher boost pressure is not accompanied by an increase in fuel flow rate, resulting in high AFR. In fact, the FI cases have a lower fuel flow rate at the same load because of the extra pump work done by the externally compressed air. Resulting FI air-fuel ratios (AFRs) vary between 57-239 and full-load AFRs vary between 57-78 relative to 23-28 for NA cases (automotive turbocharged engines generally operate between 15-30 at full load) . Note that full load shown in table 2 is defined as 12 ft-lb torque even though the torque curve is a little higher; this was necessitated by exhaust temperature limits to protect the Thermo-diluter (3200 RPM above 12 ft-lb exceeded 600^{o} C because the engine was air-cooled). Also note that the BMEP numbers for FI cases have not been adjusted to account for the pump work done by the compressed air.

Table 2. Data points used for the operating map study comprising of NA and FI cases for five loads across three engine speeds spanning the operating map (2 x 5 x 3 = 30 data pints). FI cases are shaded.

Speed	Load	BMEP	Torque	Pressure Regulator PR_2 Setting	Intake Pressure	Fuel Flow Rate	Air Flow Rate	A/F Ratio (AFR)	Exhaust Temperature
(RPM)	(Percent)	Bar	ft-lb	(PSI)	(Bar)	(kg/hr)	(kg/hr)	(None)	(Degree C)
1800	0%	0	0	NA	1.01	0.27	25	92	133
1800	25%	1.2	3	NA	1.01	0.36	24	67	181
1800	50%	2.4	6	NA	1.01	0.49	24	49	242
1800	75%	3.7	9	NA	1.01	0.65	24	37	310
1800	100%	4.9	12	NA	1.01	0.86	24	28	399
1800	0%	0	0	20	2.11	0.22	53	239	44
1800	25%	1.2	3	20	2.11	0.32	53	164	65
1800	50%	2.4	6	20	2.11	0.44	54	123	90
1800	75%	3.7	9	20	2.12	0.55	51	93	116
1800	100%	4.9	12	20	2.12	0.68	53	78	146
2500	0%	0	0	NA	1.00	0.45	35	79	178
2500	25%	3	3	NA	1.01	0.58	35	61	225
2500	50%	6	6	NA	1.00	0.77	35	45	288
2500	75%	9	9	NA	1.01	0.98	35	35	365
2500	100%	12	12	NA	1.01	1.27	34	27	458
2500	0%	0	0	20	2.01	0.39	75	192	78
2500	25%	1.2	3	20	2.02	0.54	75	140	102
2500	50%	2.4	6	20	2.01	0.70	74	106	130
2500	75%	3.7	9	20	2.02	0.89	75	84	163
2500	100%	4.9	12	20	2.02	1.07	75	70	196
3200	0%	0	0	NA	1.00	0.69	42	62	246
3200	25%	3	3	NA	1.00	0.85	43	50	298
3200	50%	6	6	NA	1.00	1.11	42	38	377
3200	75%	9	9	NA	1.00	1.40	42	30	460
3200	100%	12	12	NA	1.01	1.84	43	23	609
3200	0%	0	0	20	1.92	0.66	93	142	134
3200	25%	1.2	3	20	1.92	0.84	94	111	164
3200	50%	2.4	6	20	1.91	1.07	92	86	199
3200	75%	3.7	9	20	1.93	1.32	89	68	236
3200	100%	4.9	12	20	1.94	1.58	89	57	279

Each data point shown in Table 2 was allowed to stabilize for 10 minutes, followed by 5 minutes of data acquisition that was then averaged for use. Fuel rate was measured by recording the change of mass of the fuel reservoir sitting on a scale over that time period. Without flow meter-based measurements, it was not possible to adjust fuel rate to be identical between NA and FI. For in-cylinder data, fifty engine cycles were acquired for every data point and averaged for combustion analysis. Spectrometer data was directly supplied to the computer via USB, while all other signals were processed by National Instruments (NI) data acquisition device (DAQ). NI software LABVIEW was used to acquire all data except spectrometer data.

The exhaust temperature was measured at the exhaust port using a 'T-Junction' with the aerosol sample line. Note the low exhaust temperatures for FI operation, owing to higher in-cylinder mass. As will be discussed later, low exhaust temperature was correlated to high nucleation in the current work, and can also be used to explain nucleation-accumulation trade-offs reported in literature.

Table 3. Data points used for the Air-Fuel Ratio (AFR) sweep study at full load, comprising of four pressure regulator PR2 settings at three different engine speeds (4 x 3 = 12 data points)

Speed	Load	BMEP	Torque	PR2 Setting	Intake Pressure	Fuel Flow Rate	Air Flow Rate	A/F Ratio (AFR)	Exhaust Temperature
(RPM)	(Percent)	Bar	ft-lb	(PSI)	(Bar)	(kg/hr)	(kg/hr)	(None)	(Degree C)
1800	100	4.9	12	NA	1.01	0.86	25	29	370
1800	100	4.9	12	5	1.25	0.78	32	41	279
1800	100	4.9	12	10	1.45	0.76	37	48	234
1800	100	4.9	12	20	2.11	0.74	53	72	153
2500	100	4.9	12	NA	1.00	1.28	33	26	446
2500	100	4.9	12	5	1.24	1.18	42	36	354
2500	100	4.9	12	10	1.43	1.14	50	43	304
2500	100	4.9	12	20	2.06	1.09	75	68	203
3200	100	4.9	12	NA	1.00	1.83	43	24	583
3200	100	4.9	12	5	1.16	1.66	51	30	442
3200	100	4.9	12	10	1.27	1.65	57	35	403
3200	100	4.9	12	20	1.90	1.63	93	57	278

Table 3 shows engine operating points for the AFR sweep study in which pressure regulator was set at 5, 10 and 20 PSI during FI operation at full load for the three engine speeds. This allowed independent variation of AFR from its NA value without changing any parameter other than the slightly lower fuel rate owing to the pump work done by the compressed air. It can be seen that there is a smooth progression in AFR accompanied by a corresponding reduction in exhaust temperature.

3. Results: The results of the engine map traverse and AFR sweep at full load are presented separately, followed by in-cylinder combustion analysis for selected points. Subsequent to uncertainty analysis, all results are discussed together in section 4.

3.1 Engine Map Traverse: Forced induction (FI) at 20 PSI pressure was undertaken at three different speeds (1800 RPM, 2500 RPM, 3500 RPM) and five different loads (0%, 25%, 50%, 75%, 100%) to span operating map of the engine. **Figure 2** compares the particle concentration in the raw exhaust for natural aspiration (NA, left-hand figures) with forced induction (FI, right-hand figures) for these fifteen operating conditions. Each row corresponds to a different engine speed, and each plot shows the five loads at that speed. The AFR at each load is indicated on the legend.

All cases show a bi-modal distribution with a nucleation and accumulation mode. The third possible mode (coarse particles>1000 nm), if any, could not be measured since EEPS is designed to measure particles up to 600 nm (most engine exhaust particles fall within that range). All NA cases show a larger accumulation mode with increasing load/decreasing AFR, and a larger nucleation mode with decreasing load/increasing AFR. The FI cases on the right continue the same trend in general: increase in AFR resulting in substantial reduction in the accumulation mode relative to NA cases with some exceptions at 3200 RPM. This is consistent with reduction in smoke opacity at high AFRs. The nucleation mode increases slightly for 75% and 100% load, but shows mixed trends at lower loads. FI appears to make the nucleation mode narrower in all cases, and the resulting peaks are consistently located at 10 nm irrespective of their corresponding NA location. The nucleation mode trends probably do not affect visible smoke since the nucleation mode particles have insignificant mass and volume.

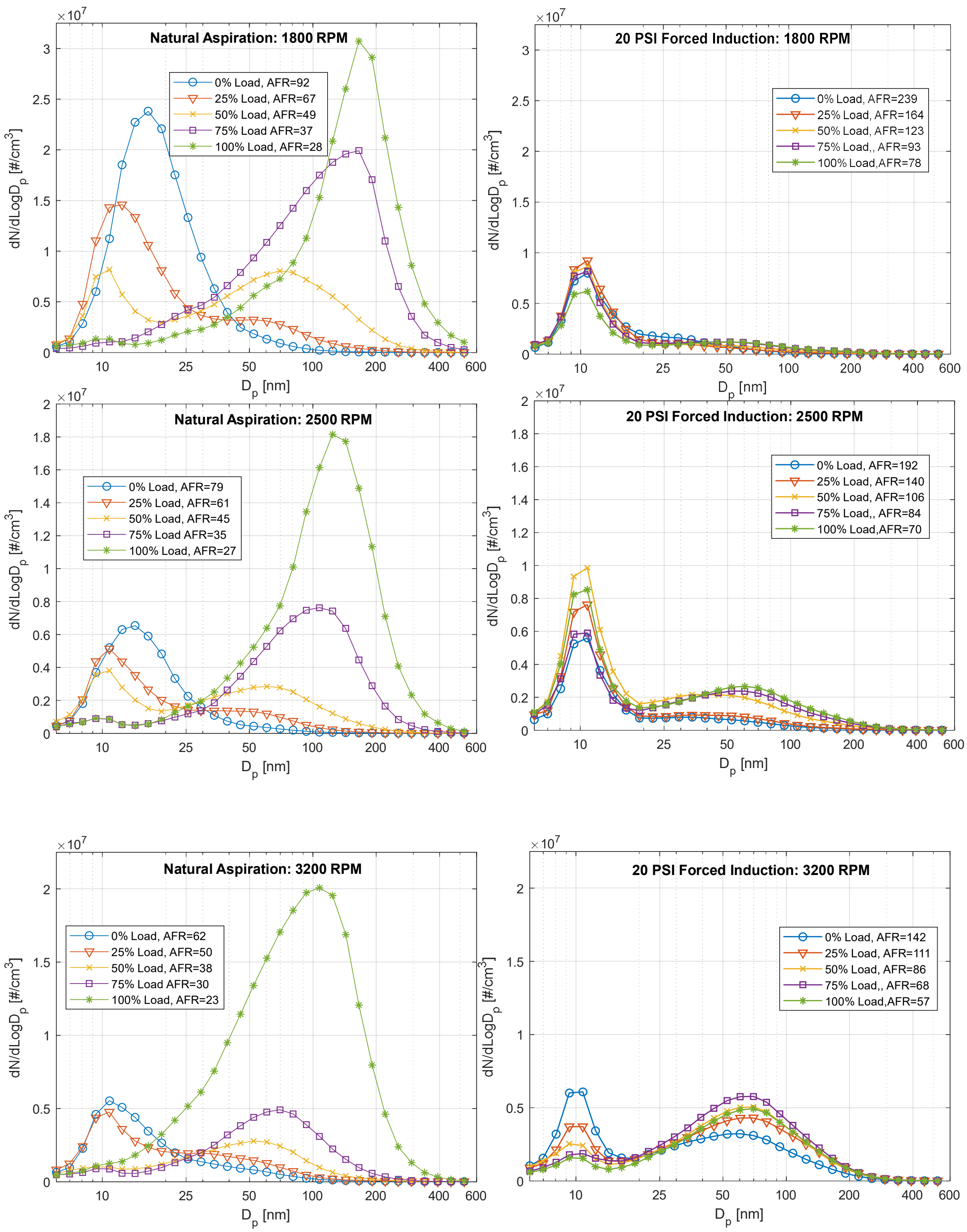

Fig 2. Particle concentration measured in the exhaust for naturally aspirated (NA, left) and forced induction (FI, right) at 20 PSI pressure for 1800 RPM (top row), 2500 RPM (middle) and 3200 RPM (bottom). FI is seen to dramatically reduce the accumulation modes at higher loads. Since FI increases exhaust flow rate, a slightly different picture emerges from plots of fuel specific particle number (FSPN), see Figure 3.

However, comparing particle concentration can be misleading. FI also increased the exhaust flow rate. Particle emission rate (PN rate) as well as fuel/brake specific PN (FSPN or BSPN) are functions of flow rate. Subsequent plots are therefore presented using a fuel specific basis (FSPN). This allows a comparison between different loads and speeds, and minimizes the effect of the discrepancy in fuel rate between NA and FI. A logarithmic scale has been used for the x-axis throughout to allow better visualization of the nucleation mode and its trade-off with the accumulation mode. Identical y-axis limits have been maintained between NA and FI at every engine speed to allow a better visual comparison.

Figure 3 shows the same results as Figure 2 but on a fuel specific basis (FSPN) instead of particle concentration. The main difference from Figure 2 is the larger size of the nucleation mode. All NA cases on the left still show higher nucleation with decreasing load/higher AFR and higher accumulation with increasing load/lower AFR. With some exceptions, the FI cases still show substantial reduction in corresponding accumulation modes but significantly higher increases in corresponding peaks of nucleation mode. At 100% load and 1800 RPM, the accumulation peak decreased about 15 times it's NA value while the nucleation peak went up by a factor of 8. Corresponding numbers at 2500 RPM were about 4 and 15, and at 3200 RPM, about 3 and 2. Hence the effect of extreme AFR's is somewhat speed dependent; at 100% load, the lowest speed produced a 15-fold reduction in the accumulation peak, the mid-speed produced a 15-fold increase in the nucleation peak, while the highest speed showed moderate trade-offs. The effects of FI at lower loads is much more moderate and they show several exceptions to the nucleation-accumulation trade-off seen at higher loads. At 0% load for example, there is a trade-off in the opposite direction. At 3200 RPM, both modes increase at lower loads. Interestingly, all FI nucleation mode peaks are narrower and more precisely centered at 10 nm relative to NA cases. Lower variation in the location of the accumulation peak is also seen.

If particle mass is estimated by assuming spherical particles with uniform density of 1 g/cm^3, then the trends for integrated fuel-specific mass (FSDPM) or brake-specific mass (BSDPM) mimic the trends in accumulation mode FSPN (since nucleation mode particles have negligible mass): but much more drastically. For example, BSDPM goes down from 0.87 g/kW-hr to 0.01 g/kW-hr for 100% load at 1800 RPM, a 62-fold reduction. BSDPM reduces by a factor of about 11 and 6 for 2500 RPM and 3200 RPM respectively. All FI BSDPM's are below 0.05 g/kW-hr. This is consistent with the disappearance of visible smoke at high AFRs. The steeper declines in BSDPM relative to FSPN peaks is attributed to the relative flattening of the PSDs at the largest diameters.

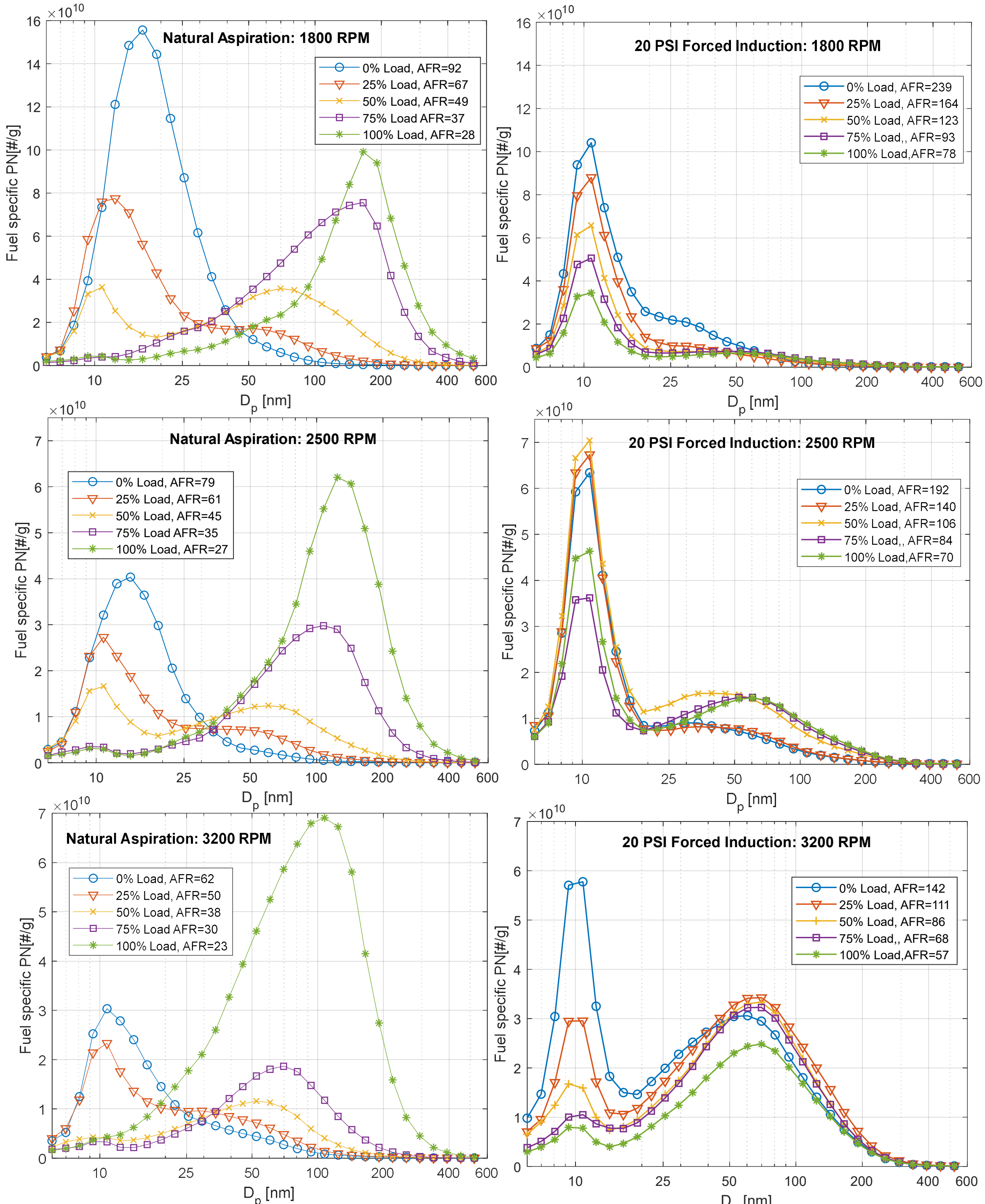

Fig 3. Fuel Specific PN per gram of fuel (FSPN) for naturally aspirated (left-hand figures) and forced induction (right-hand) at 1800 RPM (top), 2500 RPM (middle) and 3200 RPM (bottom). Higher AFRs are seen to generally reduce accumulation mode particles but increase nucleation mode particle numbers. This trade-off has a smaller magnitude at lower loads. Several exceptions exist such as 0% load at 1800 RPM and 3200 RPM .

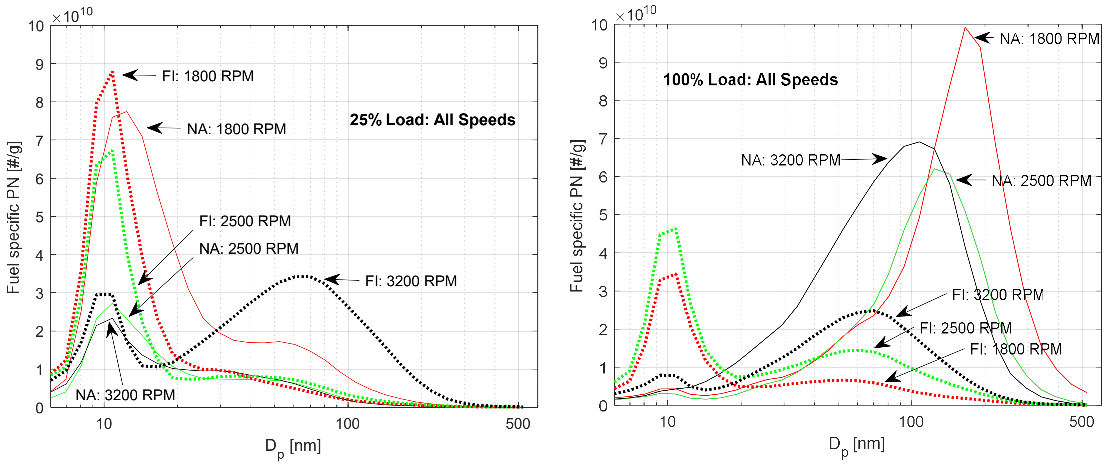

Fig 4. The 25% load (left) and 100% load results (right) of Figure 3 plotted with NA and FI on the same plot for all speeds. At 100% load, the peak of accumulation mode is speed dependent for NA but not for FI. The magnitude of increase in nucleation mode and reduction in accumulation mode caused by FI is speed dependent. The 25% case shows smaller changes for the nucleation- accumulation trade-off with an exception at 3200 RPM where both modes increase with FI.

The observations above are reiterated with **Figure 4**, which show FI (solid lines) and NA cases (dotted lines) for all engine speeds on the same plot for 25% load (left) and 100% load (right). For the 100% load plot on the right, the accumulation peak is speed-dependent for NA, but interestingly FI shifts the accumulation peaks to the left and locates them consistently within the 60-70 nm range. The degree of increased nucleation caused by FI is seen to be depend engine speed. A similar trend with smaller trade-offs is seen for the 25% load case on the left with an exception at 3200 RPM, where FI increases both modes.

Figure 5 shows integrated results to summarize the nucleation-accumulation trade-off. There is some overlap between the two modes and their locations are speed and load dependent, but 25 nm was chosen as a representative delineating particle diameter separating the accumulation and nucleation modes for illustrating the trade-off. Total FSPN below that threshold shows an increasing trend with increasing AFR (top-left), while the opposite trend (exponential drop-off) is seen for particles>25 nm (top-right) up to a certain point after which FSPN remains constant. Total FSPN for particles of all sizes (middle-left) shows mixed results due to reduced accumulation and increased nucleation and with increasing AFR, but the latter effect dominates at high AFR's because nucleation does not stop increasing with AFR. The middle-right plot shows estimated fuel specific mass (FSDPM) for all particles. The trend is similar to that of accumulation mode particles since nucleation mode particles have insignificant mass. FSDPM shows a sharper decline with AFR but stays at stable low values at high AFR'S. Estimated brake-specific mass, not shown here, had an identical trend with FSDPM reducing from 0.87 g/kW.hr at AFR~28 to about 0.01 g/kW-hr at AFR~164. The bottom plot (third row) demonstrates the trade-off directly with the nucleation mode FSPN plotted against the accumulation mode FSPN. The bottom-left corner of the trade-off (3200 RPM, 50% load) is advantageous in terms of both modes, and NA operation at 3200 RPM offers the best trade-offs in general. This observation is important for the upcoming discussion following the results section.

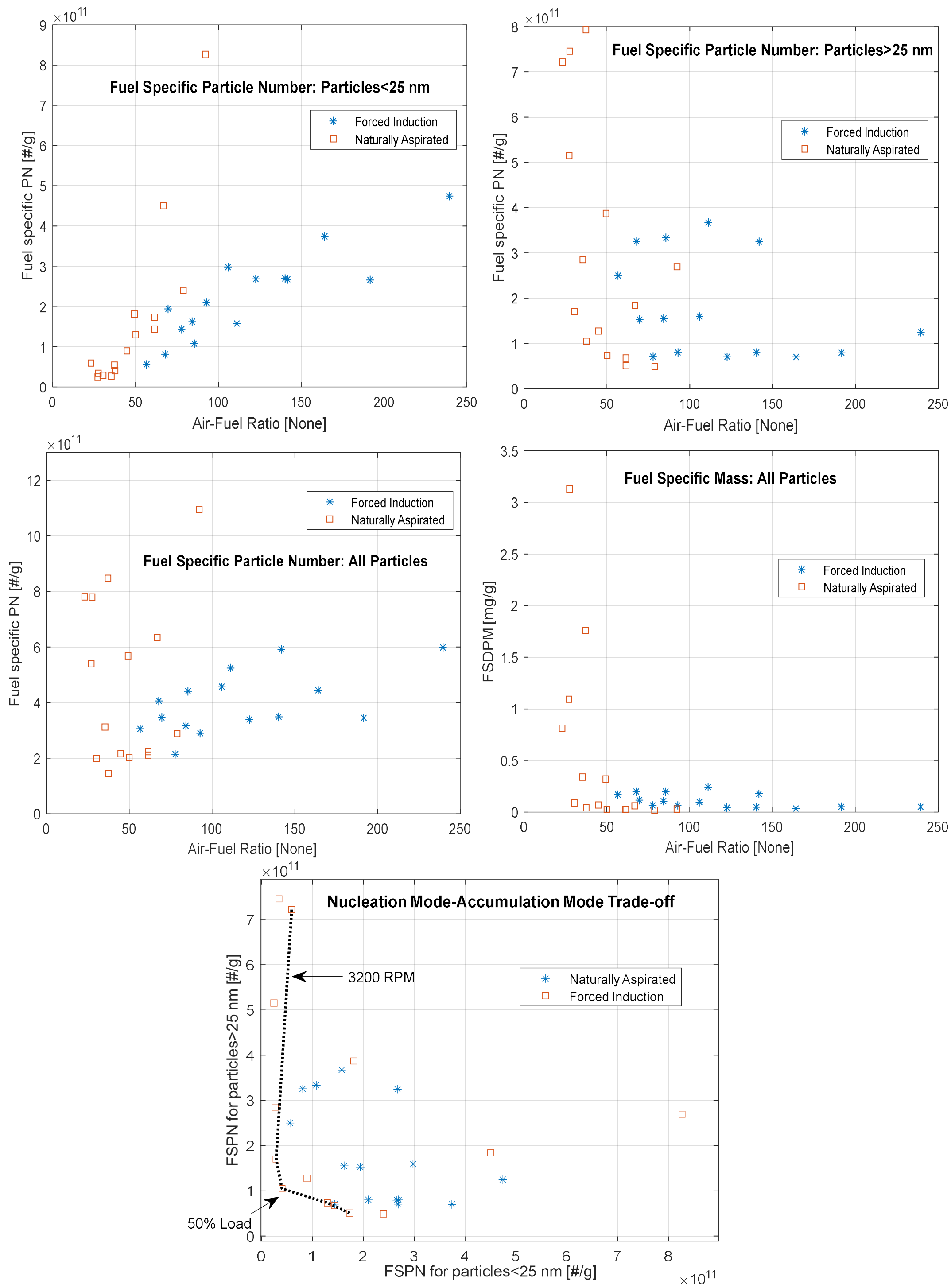

Figure 5. Integrated FSPN for particles<25 nm show a continuously increasing trend with AFR (top-left), while larger particles drop exponentially and then stay relatively constant (top-right). Integrated FSPN for all particles (middle-left) therefore show mixed trends due to this trade-off but increased nucleation at high AFR ultimately dominates because decreases in accumulation taper off. When plotted on a mass basis (middle-right), FSDPM follows similar trends as FSPN for larger particles, with a sharper initial drop-off. Bottom plot shows the direct trade-off between nucleation and accumulation mode particles. Some points with relatively low emissions of larger as well as smaller particles are marked.

3.2 AFR Sweep Results: Results presented so far show a strong relationship with AFR but are confounded with variation in load, which changes the proportion of pre-mixed and diffusion flame combustion. To isolate the effect of AFR, load was fixed at 100% and the pressure regulator setting was varied across 0 PSI, 5 PSI, 10 PSI and 20 PSI. **Figure 6** shows resulting fuel specific distributions at different speeds. The pressure setting and resulting AFRs are shown by the legend. It is seen that the nucleation mode keeps rising with higher AFR, but accumulation mode does not reduce significantly once AFR's corresponding to 5 PSI pressure is achieved. At 3200 RPM, the accumulation even increases after 10 PSI. The nucleation-accumulation trade-off is summarized by the bottom-right plot where total FSPN of particles<25 nm has been plotted against particles>25 nm. The 5 PSI points produce the lowest FSPN for both kinds of particles, since the 10 and 20 PSI points only increase nucleation without reducing accumulation significantly.

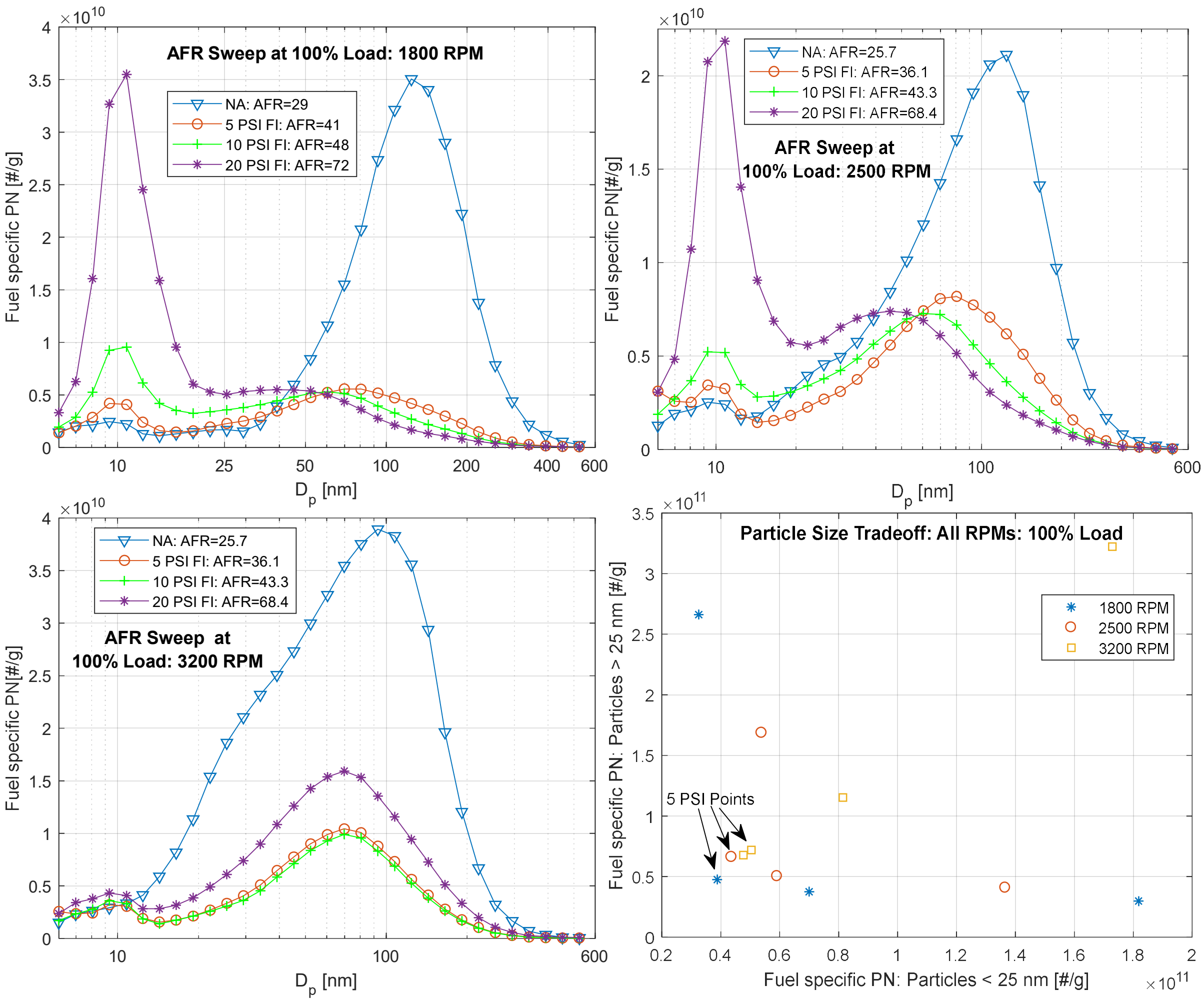

Fig 6. AFR sweep at 100% load shows continuously increased nucleation with increasing AFR at all speeds (top row and bottom left), while the accumulation mode does not significantly decrease beyond the AFRs corresponding to 5 PSI supply pressure. Therefore, when particles < 25 nm (x-axis) are plotted against particles > 25 nm (y-axis) ,bottom-right, the 5 PSI points show the lowest numbers for both kinds of particles.

Note that the AFR study was performed with a different batch of fuel than the operating map study, and the PSD's are not directly comparable. This aspect has been discussed further in the uncertainty analysis section.

3.3 In-Cylinder Analysis: In-cylinder pressure traces (average of 50 cycles) and resulting average temperatures and heat release rates are shown by **Figure 7** for 1800 RPM. Other engine speeds had the same trends. The NA and FI (at 20 PSI) plots are shown by solid and dotted lines respectively, and five traces corresponding to the five loads are shown and for both cases. The top row shows overall and zoomed-in pressure traces. FI cases are seen to produce peak cylinder pressures (PCP's) that are between 1.8 times (100% load) to 2 times (0% load) the corresponding NA PCP's, due to 2.1-2.2 times higher in-cylinder mass. The **top-right** figure zooms into the PCP region. It is seen that FI PCP's occur slightly earlier than corresponding NA PCP's, e.g. the 100% load FI PCP occurs about 3° prior to the 100% NA PCP. For both NA and FI, PCP's occur earlier at lower loads but the difference in NA PCP location and FI PCP location at the same load stays about the same.

The **mid-left** plot shows the average cylinder temperatures calculated from the pressure traces. The FI temperatures are generally somewhat higher prior to combustion, but significantly lower afterwards due to the higher in-cylinder mass. The difference between NA and FI temperature peaks increase with load because the FI peaks diverge less than NA peaks which show significant increases with load. The FI combustion starts earlier owing to lower ignition delay resulting from the significantly higher pressure. There is a brief window between -8° to -2° where FI cases have higher temperatures resulting from combustion, but are quickly overtaken after NA cases combust at around -7.2°. The **mid-right** plot compares apparent heat release rates (AHRR) calculated from the pressure and temperature traces. The location of the pre-mixed spike, as well as start of combustion (SOC) stays relatively constant across load, but ignition delay is about 5° for the FI cases and about 9° for NA cases. The large dip for the FI cases prior to SOC is due to the large negative work of compression. The magnitude of the FI pre-mixed spikes are lower because the lower ignition delay corresponds to lower mass injected till SOC. The total positive area under the AHRR curve is also approximately 15% lower for the FI cases due to the ~15% lower fuel mass per stroke. This is because of the extra pump work done by the compressed air on the engine.

The **bottom plots** show normalized AHRR and cumulative heat release (CHR) plots for 100% load (left) and 25% load (right). Both plots show a constant difference of 5° in the location of NA and FI pre-mixed peaks. For the 100% load case, the diffusion/late burn phase is 23° shorter for the FI case, partly due to less fuel injected. But the CHR curve also show a higher slope for FI during most of the diffusion burn phase suggesting faster combustion possibly due to excess Oxygen. The pre-mixed phase has similar CHR slope for FI and NA, perhaps due to excess Oxygen for both cases during that phase. A dip in AHRR and reduction of the CHR slope is seen for the FI case starting at about -4°, in between the pre-mixed and diffusion burn phase. No such dip is seen for the NA case, suggesting that there might be a delay is establishing the diffusion flame due to the lower cylinder temperature of the FI cases. The 25% case shows a more precipitous drop in AHRR and a complete flattening of the CHR slope between -5° to 3°. Unlike the 100% load case, duration of combustion is similar for FI and NA.

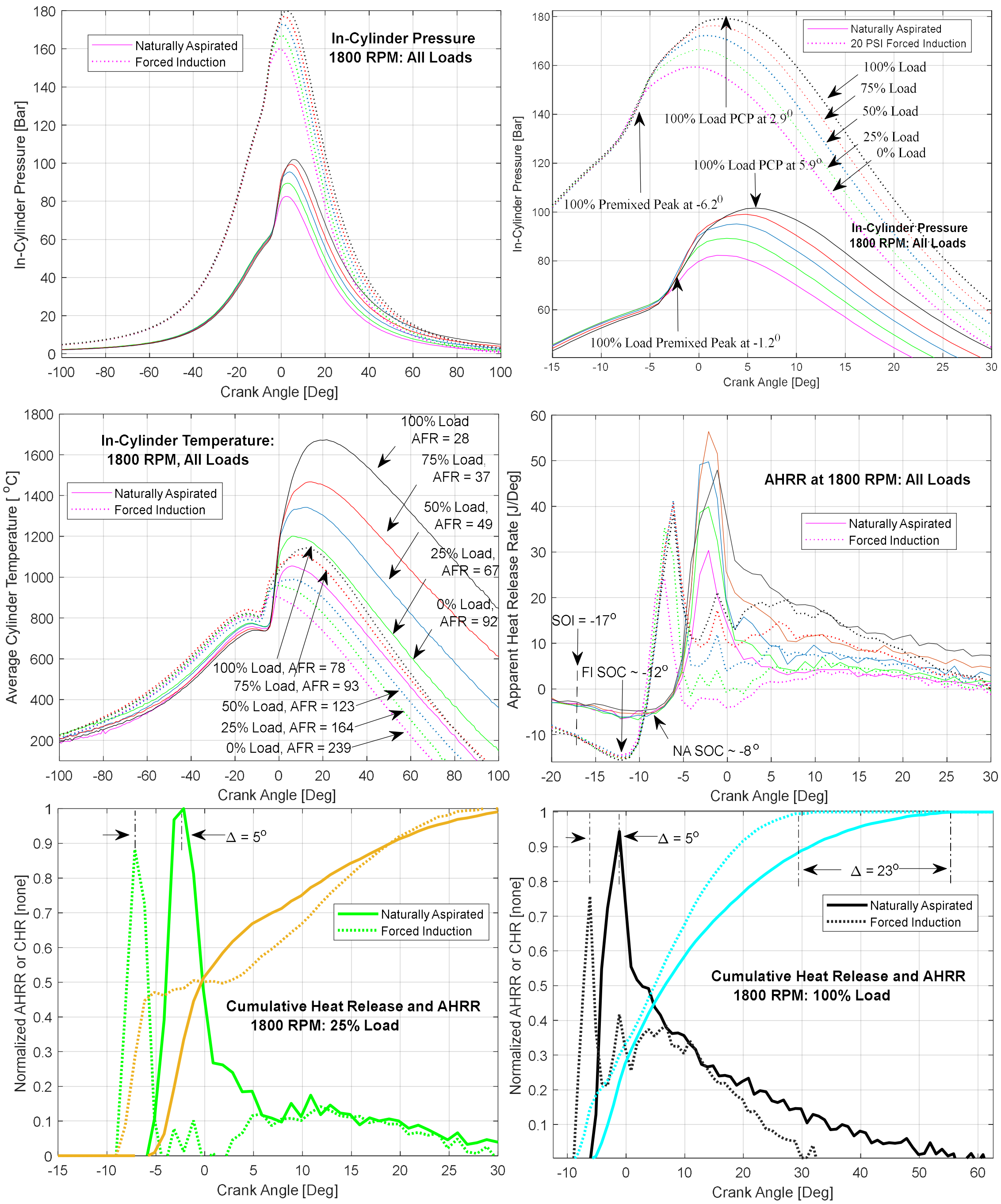

Fig 7. Top row: Pressure traces show FI achieve 1.8-2 times peak cylinder pressure of NA cases. Middle Row: FI cases have a smaller ignition delay than NA cases (right) but result in significantly lower combustion temperatures (left). Bottom: The slope of the cumulative heat release (CHR) curve is similar between FI and NA for the pre-mixed phase, but generally higher for FI during the diffusion burn phase at 25% load (left) and 100% load (right). FI cases show a flattening of burn rate between the pre-mixed and diffusion burn phase.

Overall, In-Cylinder Analysis suggests that FI cases have earlier and faster Oxygen rich combustion at lower temperatures relative to NA cases.

3.4 Uncertainty Analysis: Figure 8 shows the upper and lower bounds for NA and FI cases at 2500 RPM and 100% load, for a given batch of fuel. This operating condition was chosen as the repeat point to quantify random uncertainty, determined by using the t-distribution to find a range of population means from the repeat data. Systematic error was assumed to be 18% of the sample mean, based on comparative data between the fast-sizer and CPC counter provided by the manufacturer (TSI application notes-b). The upper and lower boundaries shown in figure 8 include both the systematic and random error. It can be seen there is no overlap between the NA and FI cases, i.e., the upper limit of FI accumulation mode is below the lower limit of NA accumulation mode, and vice-versa for the nucleation mode.

As previously mentioned, in order to eliminate variation due to fuel chemical composition, all FI and NA comparisons presented so far were made using the same fuel. However, due to storage constraints, different batches of fuel were required for the engine map traverse, AFR sweep and repeatability study discussed below.

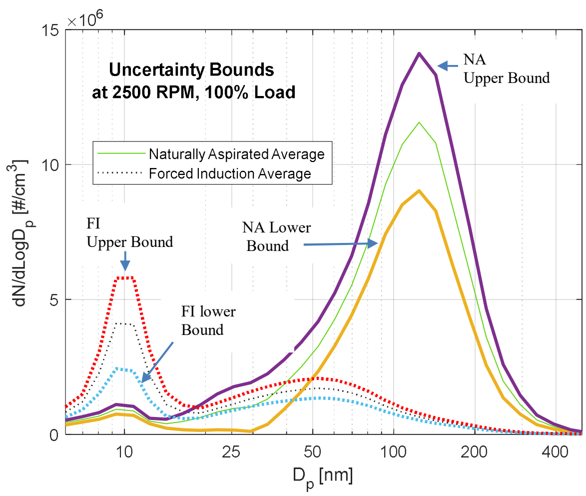

Fig 8 : No overlap between NA and FI cases is seen for uncertainty bounds calculated for the same batch of fuel. For the accumulation mode, the upper bound of FI is lower than the lower bound of NA. For the nucleation mode, the upper bound of NA is lower than the lower bound of FI. All NA and FI comparisons presented were made with the same batch of fuel, although different batches were used for different parts of the study

Figure 9 shows the repeat point recorded over a period of a one year with multiple batches of ultra-low sulfur diesel fuel procured from the gas station. Considerably more variation exceeding the uncertainty bounds of the single batch fuel is observed. Yet, there is still no overlap between any FI or NA case recorded over a time period of one year with multiple batches of fuel. This demonstrates the consistency and robustness of the nucleation- accumulation trade-off.

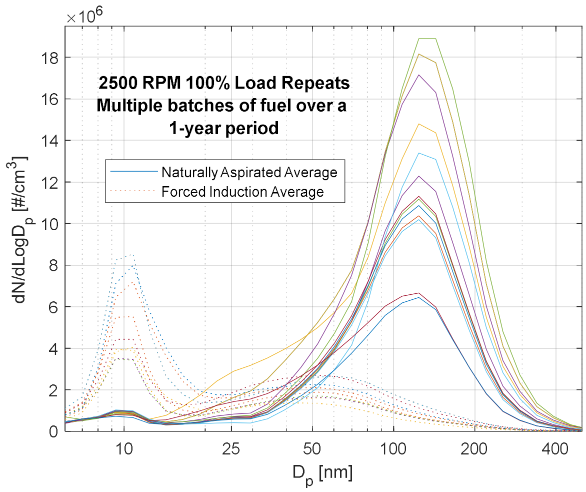

Fig 9 : No overlap between NA and FI cases is seen for the repeat data over a one-year period with different batches of fuel

There exist however, several additional uncertainties due to losses within the 4-m copper coil sample line and the EEPS measurement system. As mentioned previously, the coil was required to damp severe vibrations from the single-cylinder engine during FI operation as the in-cylinder pressure exceeded design limits (special bolts were used to secure the cylinder head). But the length of the copper coil entailed significant convective-diffusion and thermophoretic losses. The thermodiluter maintained an approximately 1 L/min flow rate through the sample line for both FI and NA operation. At constant flow rate, the diffusion losses increase with decreasing particle size, and were calculated to be as high as 40% for 10-nm particles going down to 3% at 100-nm near the accumulation peaks (Hinds, 1999), the observed peak of the FI nucleation mode. Note that diffusion losses do not affect the relative changes between NA and FI cases because of the constant flow rate through the sample line.

Thermophoretic losses due to temperature differences between bulk gas and wall temperature were calculated according to formulations proposed by Housiadas et. al., 2005, as presented in a simplified guide by Giechaskiel et. al., 2012. They increase with the temperature difference between bulk gas and wall temperature, and are almost independent of particle size for the size range of engine exhaust. For NA operation at 100% load (highest losses), thermophoretic losses were estimated to vary between 26%-34%. Corresponding FI losses were lower, ranging between 12%-21% because exhaust gas temperatures were lower. Hence these losses exaggerate the increase in nucleation mode due to FI operation.

A recent study by Giechaskiel et. al., 2019 has found some evidence of particles smaller than the detection limit of SMPS instruments that then grow in the sample line to particles in the 20-nm range, perhaps due to desorption from wall deposits. This phenomenon would tend to skew the results in the opposite direction, i.e. add nucleation particles rather than remove them.

Finally, the results were generated using the EEPS default matrix that converts measured charge distribution to size distribution. This default inversion matrix, although widely used, has been shown to disagree with more reliable SMPS measurements for non-spherical particles, see work by Xue et. al., 2015, that compares the default matrix with an improved new matrix (they report large improvements with the new matrix but also disagreements between EEPS and SMPS for exhaust with a strong nucleation mode).

Considering the combined uncertainties associated with EEPS, diffusion losses, thermophoretic losses and possible growth of nanoparticles in the sample line, the results of the current work should be confirmed by other researchers with improved measurement capabilities.

4. Discussion: The nucleation-accumulation tradeoff between NA and FI is seen for the majority of operating conditions over the engine map. Even though FI could reduce accumulation mode PN peaks by a factor of 15, it could also raise nucleation PN by the same factor. The AFR sweep results show that accumulation PN dropped sharply with increasing AFR but subsequently remained at a stable low value at high AFR. This suggests that accumulation mode particles can be significantly reduced but not eliminated with excess Oxygen. In contrast nucleation mode particles were seen to continuously increase with AFR in general, with no asymptotic behavior. Nucleation PN rate peaks were seen to vary inversely with average in-cylinder temperature peaks.

Several researchers such as Filippo and Maricq (2008) have suggested that nucleation particles can have non-volatile cores, originating possibly from pyrolyzed hydrocarbons or lube oil derived ash. Maricq (2006) and Sgro et al. (2001, 2003, 2007) have also reported non-volatile nucleation particles < 5 nm from sooting premixed flames in a laboratory. For the results presented above, based on 150° C primary dilution, 400^{0}C evaporation tube prior to secondary dilution, overall dilution ratio of 167, the manufacturer's claims about meeting volatile particle removal requirements for European regulations (TSI application notes-a) and also considering other studies exploring the effects of dilution conditions on PN measurement (Abdul-Khalek et al. 1999, Rönkkö et al. 2006), it is reasonable to assume that the majority of nucleation particles were 'solid' non-volatile particles. Previously mentioned works by Jung et al. (2003), Pirjola et al. (2015) and Kim et al. (2020) also suggest a strong influence of lubricating oil, possibly from partial combustion of the oil mist created by the piston rings.

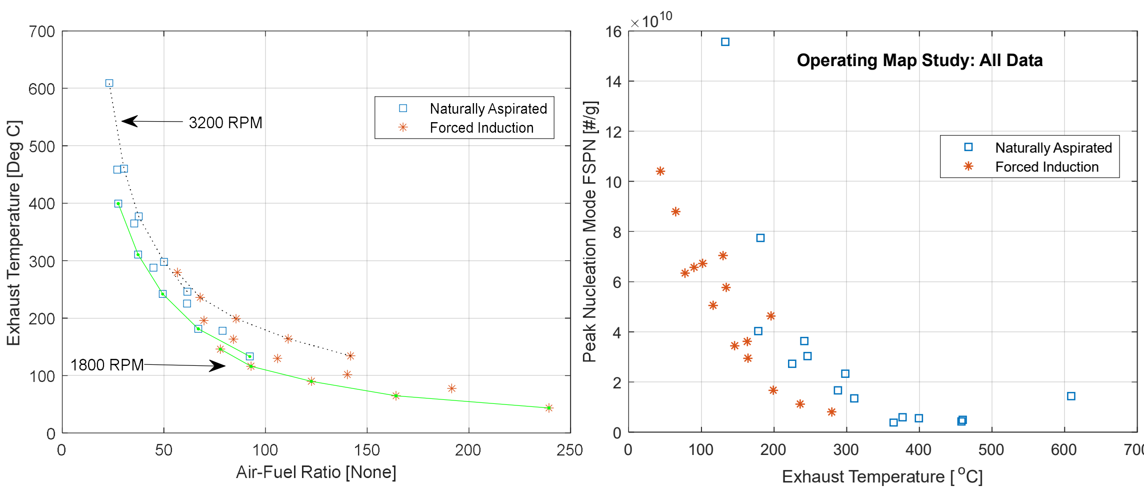

Figure 10. Peaks of the nucleation mode FSPN for the operating map study were found to be most strongly correlated to exhaust temperature

In addition to being directly correlated to AFR, the nucleation mode data in the current work was observed to be inversely correlated to exhaust gas temperature (EGT). This is easily understood by **figure 10-left**, which shows the inverse correlation between AFR and EGT. **figure 10-right** shows the FSPN nucleation peaks plotted against exhaust temperature for all FI and NA cases from the operating map study. This correlation is consistent with other studies that have reported an increasing trend of nucleation particles with increased injection pressure, advanced injection timing and lower EGR levels. All of these factors advance combustion phasing, so combustion products expand to lower exhaust temperatures across a higher effective expansion ratio. Lähde et al. (2011) reported that an increase in the injection pressure in a heavy-duty diesel engine resulted in an increase in the nonvolatile nucleation mode at medium and high loads, with no nucleation mode observed at low loads. In a separate work, Lähde et al. (2010) have reported an increase in non-volatile nucleation mode particles with decreased EGR accompanied by a reduction in accumulation mode and soot mass in a heavy-duty diesel engine. Filippo and Maricq (2008) have reported the same trend for a light-duty diesel engine. No work reporting the effect of injection timing on specifically non-volatile nucleation mode particles could be found, but many researchers have reported increased nucleation mode particles resulting from advanced timing, e.g. Benajes et al. (2012), Labecki et al. (2013), Nousiainen et al. (2013) and Wei et al. (2017). Li et al. (2014) have varied injection timing at different levels of EGR and suggested that low temperature combustion favors the nucleation mode.

Several researchers such as Xu et a. (2014 a) have investigated the morphology of particles using Transmission Electron Microscopy (TEM) and found particle size to decrease with increased injection pressure. Mathis et al. (2005) have used TEM to investigate the effect of injection pressure, injection timing and EGR on the primary soot diameter, and reported smaller diameter with higher injection pressure, advanced timing and lower EGR. They have correlated these effects to higher adiabatic flame temperature calculated from heat release rate analysis. It was suggested that higher flame temperatures caused more oxidation thus reducing particle size. However, increased nucleation resulting from higher adiabatic flame temperature, does not explain the results of the current work (FI cases do not have higher flame temperatures) or other researchers who have reported higher nucleation mode at lower loads e.g. Li et al. (2007), Gupta et al. (2010) and Srivastava et al. (2011). Instead, all of the above can be correlated to lower exhaust temperatures. Adiabatic flame temperature increases with advanced injection timing, higher injection pressure and lower EGR, all of which reduce exhaust temperatures. The previously mentioned study by Reijnders et al. (2018) is perhaps the most comprehensive investigation in the nucleation-accumulation trade-off to date. They independently varied engine load, engine speed, EGR, combustion phasing and injection pressure for 18 different fuels. They observed increased nucleation and decreased accumulation with lower load, lower speed, lower EGR, advanced combustion phasing and higher injection pressure. Each of these factors, independently varied, lowers exhaust temperature.

Reijnders et al. (2018) have discussed the 'adsorption hypothesis' to explain the nucleation-accumulation trade-off. According to this hypothesis, increased accumulation mode particles allow greater surface area for adsorption of volatile materials that are precursors of nucleation-mode particles. Any engine conditions that increase accumulation-mode particles would therefore suppress nucleation mode emissions. Reijnders et. al. have tabulated eight investigations from literature where nucleation-accumulation trade-off's have been noted. Abdul-Khalek et al. (1998), Kittelson et al. (1999), Desantes et al. (2005), Tan et al. (2014), Giechaskiel et al. (2014), Luo et al. (2015), Lattimore et al. (2016) and Qian et al. (2017) have explained their results using the adsorption hypothesis but have not provided any direct evidence.

The results of the current study could well join this list. However, based on figure 10 and the preceding discussion, it is reasonable to speculate that late-combustion temperatures might play a role in the trade-off. Higher temperatures during the late-burning phase of combustion (correlated with higher exhaust temperatures) might help oxidize nucleation particles and suppress the nucleation mode. Conversely, all factors that lower late-burning temperatures, by reducing AHRR (lower load) or advance combustion phasing (advanced timing, lower engine speed, increased rail pressure, reduced EGR) would lower temperatures during the tail-end of combustion and facilitate the nucleation mode. Note that this hypothesis is similar to the previously mentioned adiabatic flame temperature hypothesis proposed by Mathis et al. (2005), but is based on late-combustion temperatures. The adsorption hypothesis does not explain situations where both accumulation and nucleation modes reduce simultaneously, see figure 6-bottom right.

Figure 10-left shows that the 3200 RPM data has the highest exhaust temperature for the same AFR, probably owing to retarded combustion phasing at higher speed. According to the 'late-burning' hypothesis, the 3200 RPM data should have the lowest nucleation mode PN, for the same accumulation mode PN (driven by AFR). Examination of figure 5-bottom reveals that the 3200 RPM NA data is indeed located more advantageously along the trade-off than the rest of the data. A similar advantage can be seen in the work of Reijnders et al. (2018), for heptane fuels. They were shown to have the highest ignition delay relative to all other fuels. This too, can be explained by the late-burning hypothesis. But both observations are not easily explained by the adsorption hypothesis.

The role of lubricating oil in the formation of nucleation particles is clearly important. Ovaska et al. (2020) have recently reported that different lube oils produced little change in the accumulation mode but significant changes in non-volatile nucleation mode particle number. They also performed chemical analysis of the oils and reported the low particle numbers for lubricants with low Sulphur, Zinc and Phosphorous content. It is possible that lubricating oil generated ash form the core of the non-volatile nucleation particles.

Particle formation and Oxidation is a complex process that depends on the local temperature and species distribution. Although no fundamental understanding of these processes can be made from the AFRs data presented here, it can be used to calibrate the sensitivities of detailed computational models. The data is available on request. Other experimentalists are requested to confirm the correlation between exhaust/late-burning temperature and non-volatile nucleation mode emissions and design experiments with improved measurement capabilities to prove or disprove the effect of late-combustion temperatures on non-volatile nucleation particles.

From a practical point of view, engineers should be cognizant of PN emissions while adjusting AFR to meet PM or smoke limits. If the results of this work can be verified, diesel particulate filters might be the only method to reduce both kinds of emissions. Policy makers should be aware of the environmental implications of non-road diesel engines used in close proximity to humans.

5. Conclusion: Air-Fuel ratio (AFR) adjustments are widely use to limit smoke and particulate mass emissions from small non-road diesel engines. However, reduction in particulate mass (PM) can cause an increase in particle number (PN) emissions. The trade-off between larger particles comprising most of PM emissions and smaller particles comprising most of PN emissions was studied by injecting externally compressed air in a small non-road diesel engine. Particle measurements were compared between naturally aspirated (NA) and forced induction operation (FI) operation while traversing across the engine operating map. In addition, AFR sweeps were conducted at full load. It was attempted to measure only non-volatile solid particles. The following points summarize the results:

- Increased AFR due to FI operation significantly reduced accumulation mode particles (up to 15 times lower number and 60 times lower mass), but also increased nucleation mode particles by up to 15 times. Moderate AFR's produced the best trade-offs with the lowest numbers for both modes.

- Accumulation mode PN reduced sharply with increasing AFR but stayed constant beyond a certain threshold. In contrast, nucleation mode particles kept continuously increasing with increasing AFR

- In-cylinder combustion analysis revealed that increased AFR during FI operation resulted in lower ignition delay, an earlier pre-mixed spike, higher burn rates during the diffusion burn period, and lower average cylinder temperatures due to greater in-cylinder mass.

- Nucleation mode PN emissions were correlated to higher AFR's, lower average cylinder temperatures and lower exhaust temperatures. The negative correlation with exhaust temperature was found to be broadly applicable to results from other studies that have reported increases in nucleation mode particles with decreasing load, decreasing EGR, advanced timing and higher injection pressure, all of which are known to reduce exhaust temperature. It is hypothesized that nucleation mode particle numbers are oxidized at higher late-combustion temperatures and this explains the negative correlation with exhaust temperature. However, barring situations where both modes increase or decrease simultaneously, the nucleation-accumulation trade-off in the current work can still be explained by the existing 'adsorption hypothesis'.

STATEMENTS & DECLARATIONS

Funding: The EEPS Spectrometer used for this research was purchased by funds provided by grant number 1337929 from the US National Science Foundation.

Competing Interests: The authors have no relevant financial or non-financial interests to disclose.

Author Contributions: Both authors contributed to the study conception and design. The first draft of the manuscript was written by Indranil Brahma. The data was collected by Indranil Brahma and Odinmma Ofili.

Ethical Approval: Not applicable

Consent to Participate: Not applicable

Consent to Publish: Not applicable

Availability of data and materials: All results, code and raw data is available upon request

REFERENCES

Abdul-Khalek, I. S., Kittelson, D. B., & Brear, F. (1998). Diesel trap performance: Particle size measurements and trends. *SAE transactions*, 1647-1660.

Abdul-Khalek, I., Kittelson, D., & Brear, F. (1999). The Influence of Dilution Conditions on Diesel Exhaust Particle Size Distribution Measurements. *SAE transactions*, 563-571.

Benajes, J., García-Oliver, J. M., Novella, R., & Kolodziej, C. (2012). Increased particle emissions from early fuel injection timing Diesel low temperature combustion. *Fuel*, *94*, 184-190.

Bertola, A., Schubiger, R., Kasper, A., Matter, U., Forss, A. M., Mohr, M., ... & Lutz, T. (2001). Characterization of diesel particulate emissions in heavy-duty DI-diesel engines with common rail fuel injection influence of injection parameters and fuel composition. *SAE Transactions*, 1925-1937.

Brahma, I., & Chi, J. N. (2012). Development of a model-based transient calibration process for diesel engine electronic control module tables–Part 1: data requirements, processing, and analysis. *International Journal of Engine Research*, *13*(1), 77-96.

Brahma, I., & Chi, J. N. (2012). Development of a model-based transient calibration process for diesel engine electronic control module tables–Part 2: modelling and optimization. *International Journal of Engine Research*, *13*(2), 147-168.

Brahma, I. (2013). A decision-tree-based approach to smoke spike detection in a heavy-duty diesel engine. *Proceedings of the Institution of Mechanical Engineers, Part D: Journal of Automobile Engineering*, *227*(8), 1112-1129.

Brunekreef, B., & Holgate, S. T. (2002).V Air pollution and health. *The lancet*, *360*(9341), 1233-1242.

Crookes, R. J., Sivalingam, G., Nazha, M. A., & Rajakaruna, H. (2003). Prediction and measurement of soot particulate formation in a confined diesel fuel spray-flame at 2.1 MPa. *International journal of thermal sciences*, *42*(7), 639-646.

Desantes, J. M., Bermúdez, V., García, J. M., & Fuentes, E. (2005). Effects of current engine strategies on the exhaust aerosol particle size distribution from a heavy-duty diesel engine. *Journal of Aerosol Science*, *36*(10), 1251-1276.

Duvvuri, P. P., Sukumaran, S., Shrivastava, R. K., & Sreedhara, S. (2019). Modeling soot particle size distribution in diesel engines. *Fuel*, *243*, 70-78.

Englert, N. (2004). Fine particles and human health—a review of epidemiological studies. *Toxicology letters*, *149*(1-3), 235-242.

Filippo, A. D., & Maricq, M. M. (2008). Diesel nucleation mode particles: semivolatile or solid?. *Environmental science & technology*, *42*(21), 7957-7962.

Fushimi, A., Hasegawa, S., Takahashi, K., Fujitani, Y., Tanabe, K., & Kobayashi, S. (2008). Atmospheric fate of nuclei-mode particles estimated from the number concentrations and chemical composition of particles measured at roadside and background sites. *Atmospheric Environment*, *42*(5), 949-959.

Giechaskiel, B., Arndt, M., Schindler, W., Bergmann, A., Silvis, W., & Drossinos, Y. (2012). Sampling of non-volatile vehicle exhaust particles: A simplified guide. *SAE International Journal of Engines*, *5*(2), 379-399.

Giechaskiel, B., Maricq, M., Ntziachristos, L., Dardiotis, C., Wang, X., Axmann, H., ... & Schindler, W. (2014). Review of motor vehicle particulate emissions sampling and measurement: From smoke and filter mass to particle number. *Journal of Aerosol Science*, *67*, 48-86.

Giechaskiel, B. (2019). Effect of sampling conditions on the sub-23 nm nonvolatile particle emissions measurements of a moped. *Applied Sciences*, *9*(15), 3112.

Gupta, T., Kothari, A., Srivastava, D. K., & Agarwal, A. K. (2010). Measurement of number and size distribution of particles emitted from a mid-sized transportation multipoint port fuel injection gasoline engine. *Fuel*, *89*(9), 2230-2233.

He, Xin, Matthew A. Ratcliff, and Bradley T. Zigler. "Effects of gasoline direct injection engine operating parameters on particle number emissions." *Energy & Fuels* 26.4 (2012): 2014-2027.

Hinds, W. C. (1999). *Aerosol technology: properties, behavior, and measurement of airborne particles*. John Wiley & Sons.

Housiadas, C., & Drossinos, Y. (2005). Thermophoretic deposition in tube flow. *Aerosol science and technology*, *39*(4), 304-318.

Jung, H., Kittelson, D. B., & Zachariah, M. R. (2003). *The influence of engine lubricating oil on diesel nanoparticle emissions and kinetics of oxidation* (No. 2003-01-3179). SAE Technical Paper.

Kaiser, E. W., Maricq, M. M., Xu, N., & Yang, J. (2005). Detailed hydrocarbon species and particulate emissions from a HCCI engine as a function of air-fuel ratio. *SAE transactions*, 1404-1414.

Kim, K., Si, W., Jin, D., Kim, J. H., Cho, J., Baek, S., ... & Park, S. (2020). Characterization of engine oil additive packages on diesel particulate emissions. *Journal of Mechanical Science and Technology*, *34*(2), 931-939.

Kittelson, D. B. (1998). Engines and nanoparticles: a review. *Journal of aerosol science*, *29*(5-6), 575-588.

Kittelson, D. B., Arnold, M., & Watts, W. F. (1999). Review of diesel particulate matter sampling methods: Final Report. *University of Minnesota, Minneapolis, MN*, *63*.

Labecki, L., Lindner, A., Winklmayr, W., Uitz, R., Cracknell, R., & Ganippa, L. (2013). Effects of injection parameters and EGR on exhaust soot particle number-size distribution for diesel and RME fuels in HSDI engines. *Fuel*, *112*, 224-235.

Lähde, T., Rönkkö, T., Virtanen, A., Solla, A., Kytö, M., Söderström, C., & Keskinen, J. (2010). Dependence between nonvolatile nucleation mode particle and soot number concentrations in an EGR equipped heavy-duty diesel engine exhaust. *Environmental science & technology*, *44*(8), 3175-3180.

Lähde, T., Rönkkö, T., Happonen, M., Söderström, C., Virtanen, A., Solla, A., ... & Keskinen, J. (2011). Effect of fuel injection pressure on a heavy-duty diesel engine nonvolatile particle emission. *Environmental science & technology*, *45*(6), 2504-2509.

Lapuerta, M., Martos, F. J., & Herreros, J. M. (2007). Effect of engine operating conditions on the size of primary particles composing diesel soot agglomerates. *Journal of aerosol science*, *38*(4), 455-466.

Lattimore, T., Herreros, J. M., Xu, H., & Shuai, S. (2016). Investigation of compression ratio and fuel effect on combustion and PM emissions in a DISI engine. *Fuel*, *169*, 68-78.

Leidenberger, U., Mühlbauer, W., Lorenz, S., Lehmann, S., & Brüggemann, D. (2012). Experimental studies on the influence of diesel engine operating parameters on properties of emitted soot particles. *Combustion science and technology*, *184*(1), 1-15.

Li, X., Huang, Z., Wang, J., & Zhang, W. (2007). Particle size distribution from a GTL engine. *Science of the total environment*, *382*(2-3), 295-303.

Li, X., Xu, Z., Guan, C., & Huang, Z. (2014). Effect of injection timing on particle size distribution from a diesel engine. *Fuel*, *134*, 189-195.

Lu, T., Cheung, C. S., & Huang, Z. (2012). Effects of engine operating conditions on the size and nanostructure of diesel particles. *Journal of Aerosol Science*, *47*, 27-38.

Luo, Y., Zhu, L., Fang, J., Zhuang, Z., Guan, C., Xia, C., ... & Huang, Z. (2015). Size distribution, chemical composition and oxidation reactivity of particulate matter from gasoline direct injection (GDI) engine fueled with ethanol-gasoline fuel. *Applied Thermal Engineering*, *89*, 647-655.

Maricq, M. M. (2006). A comparison of soot size and charge distributions from ethane, ethylene, acetylene, and benzene/ethylene premixed flames. *Combustion and Flame*, *144*(4), 730-743.

Mathis, U., Mohr, M., Kaegi, R., Bertola, A., & Boulouchos, K. (2005). Influence of diesel engine combustion parameters on primary soot particle diameter. *Environmental science & technology*, *39*(6), 1887-1892.

Mohiuddin, K., Kwon, H., Choi, M., & Park, S. (2021). Effect of engine compression ratio, injection timing, and exhaust gas recirculation on gaseous and particle number emissions in a light-duty diesel engine. *Fuel*, *294*, 120547.

Montajir, R. M., Kawai, T., Goto, Y., & Odaka, M. (2005). *Thermal conditioning of exhaust gas: potential for stabilizing diesel nano-particles* (No. 2005-01-0187). SAE Technical Paper.

Mühlbauer, W., Leidenberger, U., Lorenz, S., & Brüggemann, D. (2013). Optical studies about the influence of diesel engine operating parameters on the physicochemical properties of emitted soot particles. *SAE International Journal of Engines*, *6*(3), 1866-1876.

Nousiainen, P., Niemi, S., Rönkkö, T., Karjalainen, P., Keskinen, J., Kuuluvainen, H., ... & Saveljeff, H. (2013). *Effect of injection parameters on exhaust gaseous and nucleation mode particle emissions of a Tier 4i nonroad diesel engine* (No. 2013-01-2575). SAE Technical Paper.

Pope III, C. A., & Dockery, D. W. (2006). Health effects of fine particulate air pollution: lines that connect. *Journal of the air & waste management association*, *56*(6), 709-742.

Ristovski, Z. D., Miljevic, B., Surawski, N. C., Morawska, L., Fong, K. M., Goh, F., & Yang, I. A. (2012). Respiratory health effects of diesel particulate matter. *Respirology*, *17*(2), 201-212.

Rönkkö, T., Virtanen, A., Vaaraslahti, K., Keskinen, J., Pirjola, L., & Lappi, M. (2006). Effect of dilution conditions and driving parameters on nucleation mode particles in diesel exhaust: Laboratory and on-road study. *Atmospheric Environment*, *40*(16), 2893-2901.

Sydbom, A., Blomberg, A., Parnia, S., Stenfors, N., Sandström, T., & Dahlen, S. E. (2001). Health effects of diesel exhaust emissions. *European Respiratory Journal*, *17*(4), 733-746.

Oberdörster, G., Sharp, Z., Atudorei, V., Elder, A., Gelein, R., Kreyling, W., & Cox, C. (2004). Translocation of inhaled ultrafine particles to the brain. *Inhalation toxicology*, *16*(6-7), 437-445.

Oberdörster, G., Oberdörster, E., & Oberdörster, J. (2005). Nanotoxicology: an emerging discipline evolving from studies of ultrafine particles. *Environmental health perspectives*, *113*(7), 823-839.

Ovaska, T., Niemi, S., Sirviö, K., Nilsson, O., Karjalainen, P., Rönkkö, T., ... & Keskinen, J. (2020). *Role of Lubricating Oil Properties in Exhaust Particle Emissions of an Off-Road Diesel Engine* (No. 2020-01-0386). SAE Technical Paper.

Pirjola, L., Karjalainen, P., Heikkila, J., Saari, S., Tzamkiozis, T., Ntziachristos, L., ... & Ronkko, T. (2015). Effects of fresh lubricant oils on particle emissions emitted by a modern gasoline direct injection passenger car. *Environmental science & technology*, *49*(6), 3644-3652.

Qian, Y., Zhang, Y., Wang, X., & Lu, X. (2017). Particulate matter emission characteristics of a reactivity controlled compression ignition engine fueled with biogas/diesel dual fuel. *Journal of Aerosol Science*, *113*, 166-177.

Reijnders, J., Boot, M., & de Goey, P. (2018). Particle nucleation-accumulation mode trade-off: A second diesel dilemma?. *Journal of Aerosol Science*, *124*, 95-111.

Rissler, J., Swietlicki, E., Bengtsson, A., Boman, C., Pagels, J., Sandström, T., ... & Löndahl, J. (2012). Experimental determination of deposition of diesel exhaust particles in the human respiratory tract. *Journal of Aerosol Science*, *48*, 18-33.

Roessler, D. M., Faxvog, F. R., Stevenson, R., & Smith, G. W. (1981). Optical properties and morphology of particulate carbon: Variation with air/fuel ratio. In *Particulate Carbon* (pp. 57-89). Springer, Boston, MA.

Sgro, L. A.; Minutolo, P.; Basile, G.; D'Alessio, A. UV-visible spectroscopy of organic carbon particulate sampled from ethylene/air flames. *Chemosphere* 2001, *42*, 671–680.

Sgro, L. A.; Basile, G.; Barone, A. C.; D'Anna, A.; Minutolo, P.; Borghese, A.; D'Alessio, A. Detection of combustion formed nanoparticles. *Chemosphere* 2003, *51*, 1079–1090.

Sgro, L. A.; De Filippo, A.; Lanzuolo, G.; D'Alessio, A. Characterization of nanoparticles of organic carbon (NOC) produced in rich premixed flames by differential mobility analysis. *Proc.Combust. Inst.* 2007, *31*, 631–638.

Srivastava, D. K., Agarwal, A. K., & Gupta, T. (2011). Effect of engine load on size and number distribution of particulate matter emitted from a direct injection compression ignition engine. *Aerosol and Air Quality Research*, *11*(7), 915-920.

Tan, P. Q., Ruan, S. S., Hu, Z. Y., Lou, D. M., & Li, H. (2014). Particle number emissions from a light-duty diesel engine with biodiesel fuels under transient-state operating conditions. *Applied Energy*, *113*, 22-31.

TSI EEPS 3090 application notes for calibration of volatile particle removal system: https://tsi.com/getmedia/e119812b-1cfa-4b13-8dfb-6656ee75d4d7/EM-003-Explaining_VPR_Calibration-5001327A?ext=.pdf

TSI EEPS 3090: https://tsi.com/products/particle-sizers/particle-size-spectrometers/engine-exhaust-particle-sizer-spectrometer-eeps-3090/

TSI EEPS 3090 application notes for reproducibility: https://tsi.com/getmedia/c3524b79-87a7-47f7-ad87-e08929000369/EEPS_Reproducibility_App_Note_EEPS-008_US-web?ext=.pdf

US EPA Tier 4 standards: https://dieselnet.com/standards/us/nonroad.php#tier4

Wei, M., Li, S., Liu, J., Guo, G., Sun, Z., & Xiao, H. (2017). Effects of injection timing on combustion and emissions in a diesel engine fueled with 2, 5-dimethylfuran-diesel blends. *Fuel*, *192*, 208-217.

World Bank: **Diesel power generation: inventories and black carbon emissions in Nigeria** [Online]. Available: http://documents.worldbank.org/curated/en/853381501178909924/pdf/117772-WP-PUBLIC-52p-Report-DG-Set-Study-Nigeria.pdf (2014), Accessed 17th May 2022
Google Scholar

Xu, Z., Li, X., Guan, C., & Huang, Z. (2014). Effects of injection pressure on diesel engine particle physio-chemical properties. *Aerosol Science and Technology*, *48*(2), 128-138.

Xu, Z., Li, X., Guan, C., & Huang, Z. (2014). Effects of injection timing on exhaust particle size and nanostructure on a diesel engine at different loads. *Journal of aerosol science*, *76*, 28-38.

Xue, J., Li, Y., Wang, X., Durbin, T. D., Johnson, K. C., Karavalakis, G., ... & Jung, H. S. (2015). Comparison of vehicle exhaust particle size distributions measured by SMPS and EEPS during steady-state conditions. *Aerosol Science and Technology*, *49*(10), 984-996.

Xue, J., Hu, S., Quiros, D., Ayala, A., & Jung, H. S. (2019). How do particle number, surface area, and mass correlate with toxicity of diesel particle emissions as measured in chemical and cellular assays?. *Chemosphere*, *229*, 559-569.

Yamada, H., Misawa, K., Suzuki, D., Tanaka, K., Matsumoto, J., Fujii, M., & Tanaka, K. (2011). Detailed analysis of diesel vehicle exhaust emissions: Nitrogen oxides, hydrocarbons and particulate size distributions. *Proceedings of the Combustion Institute*, *33*(2), 2895-2902.

Zhu, J., Lee, K. O., Yozgatligil, A., & Choi, M. Y. (2005). Effects of engine operating conditions on morphology, microstructure, and fractal geometry of light-duty diesel engine particulates. *Proceedings of the Combustion Institute*, *30*(2), 2781-2789.